Hydrophilic and super hydrophilic self-cleaning coating by morphologically varying

ZnO microstructures for photovoltaic and glazing application

Srijita Nundy[1], Aritra Ghosh[2*], Tapas K Mallick[2]

[1]School of advanced materials science and engineering, Sungkyunkwan University, Suwon 16419, Republic of Korea

[2]Environmental and Sustainability Institute, University of Exeter, Penryn, Cornwall, TR10 9FE, UK

*Corresponding author: a.ghosh@exeter.ac.uk; aritraghosh_9@yahoo.co.in

Abstract:

Transparent, super-hydrophilic materials are indispensable for their self-cleaning function which has become an increasingly popular research topic, particularly in photovoltaic (PV) applications. Here, we report hydrophilic and super hydrophilic ZnO by varying morphology to employ as a self-cleaning coating for PV application. Three different ZnO microstructures such as ZnO nanorods (R-ZnO), ZnO microflower (F-ZnO), ZnO microspheres (M-ZnO), were developed by hydrothermal methods. The surface morphology by using X-ray diffraction (XRD), wettability behaviour by using water contact angle (WCA), structural, and optical properties by using Photoluminescence (PL), Raman and UV-Vis spectrophotometer, defects estimation by using XPS of the ZnO nanostructured films were systematically investigated. XRD confirmed the formation of the hexagonal wurtzite structure of ZnO. The average crystallite size of prepared R-ZnO, F-ZnO, M-ZnO, were found to be 28.95 nm, 11.19 nm, and 41.5 nm, respectively. The bandgap of ZnO nanostructures was calculated from the UV–vis absorption spectrum and found to be 3.6 eV, 3.3 eV and 3.1 eV for R-ZnO, F-ZnO, and M-ZnO respectively. WCA for R-ZnO and F-ZnO had 20.2°, 11.19° respectively while M-ZnO behaved liked super hydrophilic having WCA of 2.8°.

Keywords: ZnO, super hydrophilic, hydrophilic, PV, flower, nanorods, microsphere, glazing

1. Introduction

Deposited dust or organic contaminant on photovoltaic (PV) glass cover reduces solar photon flux reaching a PV cell via spectral absorption and reflection losses. This optical loss reduces PV power which can vary between 2% to 50% depending on local climate, dust composition, dust particle concertation, surface morphology of PV glass and employed dust mitigation techniques [1,2]. Prominent dust impact on PV module is found in arid or semi-arid areas, such as the Middle East and North Africa and in most cleaned area UK was up to 5% soiling losses is possible due to dust accumulation. PV

31 installed capacity in the world is likely to be more than doubled in a few years, and PV is installed faster

32 than any other renewable energy technologies. Thus, the effect of the dust deposition to improve the

33 PV system efficiency is significant.

34 Manual, automated, electrostatic, electrodynamic and self-cleaning are the different applied techniques

35 to clean a soiled PV device. Except for self-cleaning, other types are time-consuming, costly, and

36 hazardous to the environment and corrode the solar panel frame [3]. Two different self-cleaning methods

37 are presently available which includes either photocatalytic hydrophilic or hydrophobic types [4]. The

38 hydrophobic coated surface shows water contact angle $\geq 90°$ and low surface energy while hydrophilic

39 coated shows contact angles $\leq 90°$ and high surface energy [5]. Water contact angle (WCA) greater than

40 150^0 shows super hydrophobic property whereas less than 5^0 shows a super hydrophilic property[6,7].

41 Suspended water, dirt or any pollutant roll down spontaneously due to non-equilibrium thermodynamic

42 state from a super hydrophobicity surface[4,8,9]. They are also capable to reduce formation of corrosion

43 and ice and drag reduction. On the other hand, hydrophilic and super hydrophilic surface spreads water

44 droplets to form a film throughout itself, thereby, allows light waves to pass through and diminish any

45 pollutants through photocatalysis reaction. For anti-soling purpose super hydrophilic provides 2.5 times

46 higher efficiency compared to superhydrophobic coating [10,11]. The wetting behaviour of hydrophobic

47 and hydrophilic coating is a combined effect of its surface topography and microstructure, surface free

48 energy, and the chemical composition. Semi conductive metal oxide has ability to perform as self-

49 cleaning coating.

50 Zinc oxide is one of the important semiconductors, often selected as a doped material due to its wide

51 bandgap of 3.37 eV with a large excitation binding energy of 60 meV, low cost, non-toxic, optical and

52 photochemical properties. ZnO surfaces display better photocatalytic performance in the degradation

53 of hazard dye molecules in both basic and acidic medium. Also, ZnO is bio-safe and biocompatible and

54 thus environmentally benign coating [12]. Zinc oxide has been extensively investigated due to its

55 promising applications in short-wavelength lasing, gas sensors [13], catalysts [14], PV cells [15], transparent

56 conductors [16], and piezoelectric materials [17], photodiode [18], transistor [19], varistor [20]. ZnO nanostructures

57 have been synthesized in different morphologies such as nanowire arrays [21,22], nanorods [23], nanotubes

58 and nanoflowers, nanosheets [24] using physical and chemical methods for self-cleaning application.

59 Various techniques have been utilizing to prepare ZnO nanostructured films for self-cleaning

60 applications such as magnetron sputtering [25], spray pyrolysis, thermal oxidation, reactive evaporation

61 [22], vapor phase epitaxy, electrodeposition, sol-gel [26], solid-state reaction and, chemical deposition [27].

62 However, to support the high demand for low-cost mass production of hydrophobic/hydrophilic ZnO

63 nanostructured surfaces for PV application hydrothermal process is efficient. ZnO nanostructure

64 prepared by hydrothermal methods has excellent crystalline quality, high surface area, chemical, and

65 thermal stability, low growth temperature and environmentally safe (water used as a solvent) with a

66 strong possibility of scaling up [26].

67 The surface of ZnO can be hydrophobic or hydrophilic depending upon physical and chemical

68 properties of ZnO/water interfacial interactions. ZnO is introduced to prepare superhydrophobic with

69 WCA of 158° and a sliding angle of about 6° Zn coating on steel substrate [24]. ZnO hydrophobic coating

70 was prepared on borosilicate glass, amorphous Quartz, single crystal sapphire, lanthanum aluminate

71 and yttria-stabilized zirconia substrates using thermal evaporation methods [22] which were also suitable

72 for mechanical and oxidation resistance applications. Flexible self-cleaning nanofiber membrane using

73 oleic acid-coated ZnO nanowire structure had WCA $>150^0$ which closely resembled the nanoscale

74 tubular randomly oriented crystalloids on lotus leaf [21].

75 Pesika et al. reported that the surface of a ZnO single crystal is relatively hydrophilic [28]. Photocatalytic

76 self-cleaning ZnO on cellulosic fibres were prepared by ambient temperature sol-gel process [26].

77 Composite ZnO /TiO$_2$ film possesses super hydrophilicity with a water contact angle of less than 5°

78 without UV irradiation [29].

79 Switching wettability by the transformation between oxygen vacancy state (hydrophobic) and oxygen-

80 rich (hydrophilic) state is possible with ZnO [30]. The transition between hydrophilicity to super

81 hydrophobicity of transparent ZnO nanorod array films was prepared by a hydrothermal method which

82 was highly hydrophilic with a water contact angle of 9.6±0.8°. Superhydrophobic was achieved with a

83 water contact angle of 156.2±1.8 after being exposed to octa decanethiol solution [23]. ZnO shows

84 hydrophobic and super hydrophobicity at normal conditions which can be UV cured to obtain

85 hydrophilic property [31].

86 The surface roughness of hydrophobic and superhydrophobic surface can limit the transparency of that

87 surface. Surface roughness higher than one-quarter of a wavelength of a visible hindrance to achieving

88 transparency in visible light [32–34]. However, for PV application transparent self-cleaning coating is

89 paramount.

90 In this contribution, we describe a facile synthesis of morphologically varied hydrophilic and super

91 hydrophilic ZnO microstructures without UV treatment for self-cleaning techniques of PV and glazing

92 applications. ZnO micro flower, nanorod, and microspheres were developed on the ITO glass substrate.

93 ## 2. Results and Discussion

94 ### 2.1. Morphological analysis

95

96 The **XRD** profile of as-prepared samples is represented in Figure 1, revealed that all the diffraction

97 peaks are indexed to the hexagonal wurtzite structure of ZnO (space group P63*mc*, JCPDS Card Number

98 36-1451) ensuring its identity. The sharp diffraction peaks indicate good crystallinity. Using Scherrer's

99 equation $D = \dfrac{K\lambda}{\beta \cos\theta}$, the crystallite size of the R-ZnO, F-ZnO, and M-ZnO was calculated to be

100 41.5 nm, 28.95 nm, 11.19 nm and respectively.
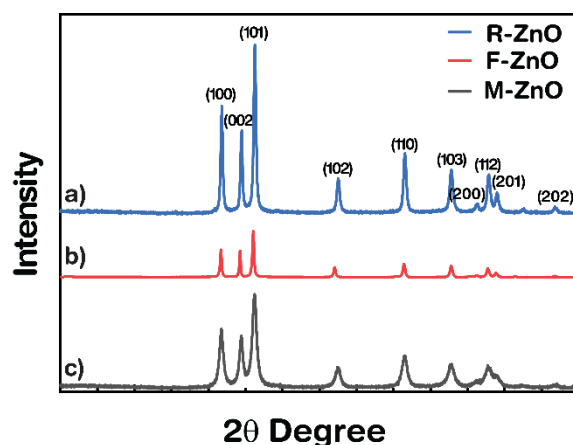
Figure 1: XRD pattern of as-synthesized samples of ZnO (a) Nanorods (R-ZnO) (b) Flower-like (F-ZnO) and (c) Porous Microsphere (M-ZnO).

Figure 2 (a-c) displays the **FE-SEM** micrographs of the three different morphologies of as-prepared ZnO microstructures. The FE-SEM analysis revealed the growth of as grown nanorods R-ZnO, rod assembled flower-like F-ZnO and porous microsphere M-ZnO can be varied by merely changing surfactant, hydrothermal reaction conditions and calcination process. ZnO has a tendency of forming rods as the growth is dominated unidirectionally, thereby forming rod-shaped morphology of the ZnO (Figure 2a). CTAB on the other hand behaves not only as a growth promoter but also as a soft template for the formation of flower-like morphology of ZnO by providing active sites (CTAB-conjugated growth units) along the circumference of ZnO nuclei which help in the adsorption of growth units and altering its surface energy eventually allowing the low-temperature radial growth of uniformly distributed F-ZnO microstructures (Fig. 2b). The uniformly distributed individual crystalline nanorods were ~1 µm long with an average diameter of 20 nm. The flower-like sample having a diameter ranging from 2 µm. By changing the surfactant to urea with subsequent calcination of the ZHC precursor the ZnO microspheres were formed with highly porous nanosheets. The decomposition of ZHC resulted in evaporation of H_2O and CO_2 during calcination resulting in formation of ZnO with porous surface (Figure 2c). All three samples maintained their morphologies even after undergoing aging with post-annealing at 350°C on the glass substrate as shown in Figure 2(d-f).
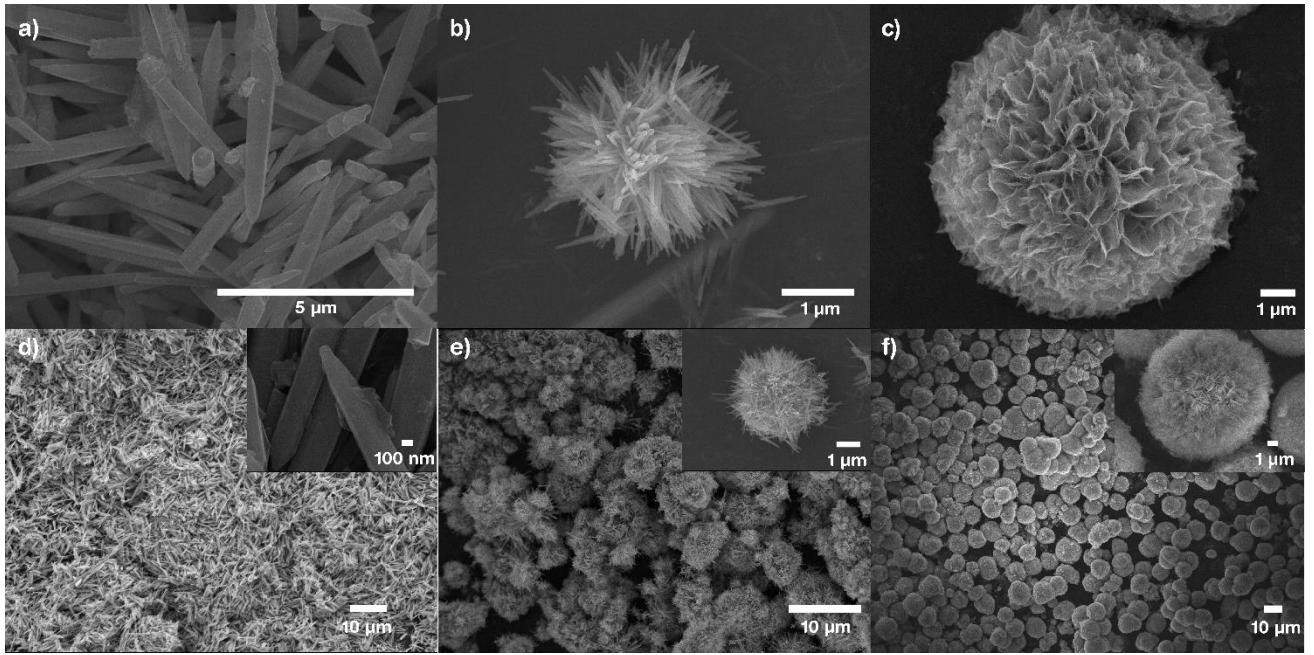
Figure 2: FE-SEM images: before annealing (a) R-ZnO, (b) F-ZnO, and (c) M-ZnO and on device after annealing at 350°C (d) R-ZnO, (e) F-ZnO, and (f) M-ZnO

2.2. Wettability property by contact angle measurements and optical property analysis

The images obtained for determination of water contact angle (WCA) along with the shape of water droplets formed on the surface are shown in detail in Figure 3 for R-ZnO, F-ZnO, and M-ZnO. The WCA was found to be 20.2°, 11.19° and 2.8° for surfaces with R-ZnO, F-ZnO, and M-ZnO respectively. All contact angles were measured with a 5 µL water droplet at ambient temperature. The results clearly indicate hydrophilic surfaces for rods and super hydrophilic in case of flowers and microspheres assembled surfaces. These results could arise due to the crystallinity and microstructural changes that occur by the synthesis of these microstructures. Due to the abundance in the number of troughs between the microstructures, the surface's roughness is increased, and the wettability is largely affected thereby following Wenzel's model.
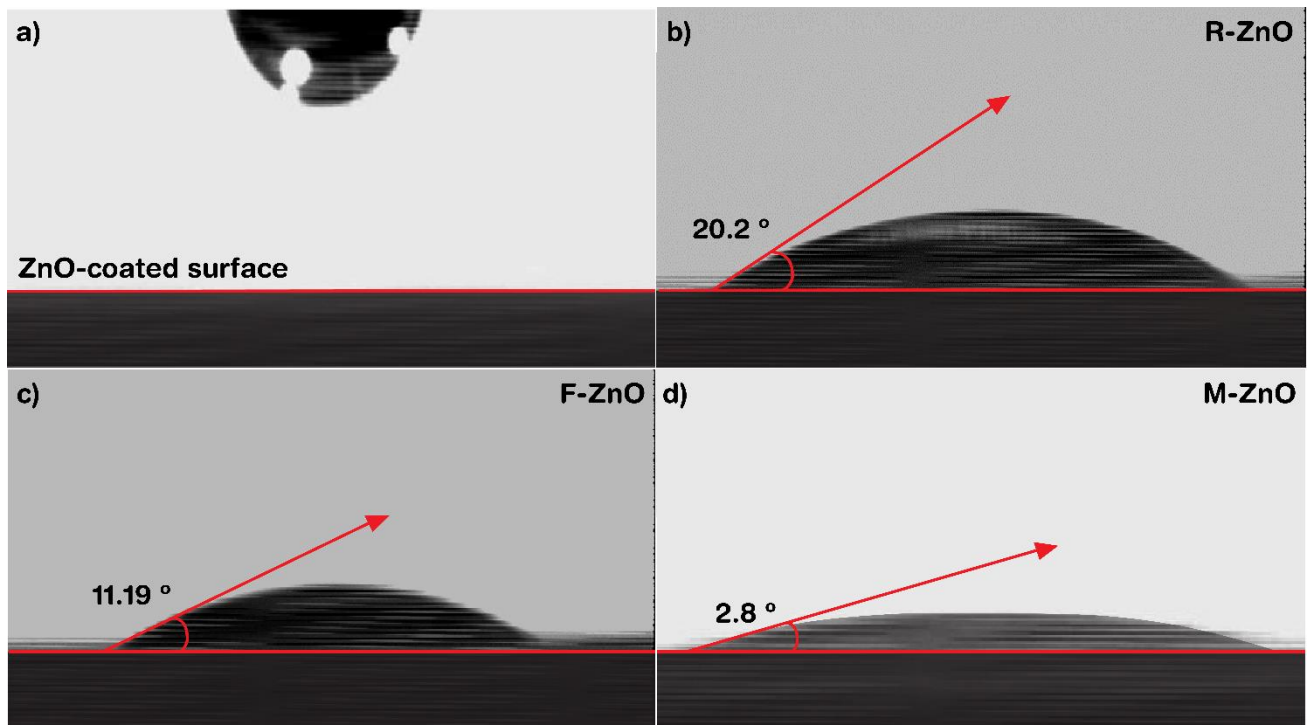
Figure 3: Water droplet contact angle measurement: (a) waterdrop before contacting with the surface and after contacting the ZnO coated glass substrate (b) nanorods (R-ZnO) (c) micro flowers (F-ZnO) and (d) porous microspheres (M-ZnO).

2.3. Optical property analysis

The optical transmission and absorption behaviour of different ZnO morphologies fabricated on the glass substrate was observed by using **UV-Vis-NIR** spectroscopy analysis as shown in Figure 4. Band gaps of R-ZnO, F-ZnO, and M-ZnO were obtained by calculation from the tauc-plot as 3.6, 3.3 and 3.1 eV. The slight shifting in bandgap arises due to a change in morphologies, defects and grain size. It was clearly hinted that the morphology of the microstructures could efficiently control the transmittance, absorbance and optical bandgap. Reduced band gap can enhance its electrical property, thereby decreasing resistance. V_0 acts as electron donor forms acceptor states near the valence band. When the concentration of the V_0 is high enough, V_0 states overlap with the valence band pushing it upwards towards the conduction band. With increase in V_0 there is an increase in the number of energy states above the valence band and hence increases the bandgap narrowing. Thus, in our case, various morphologies of ZnO display different energy band gap values because they have different concentrations of V_0.
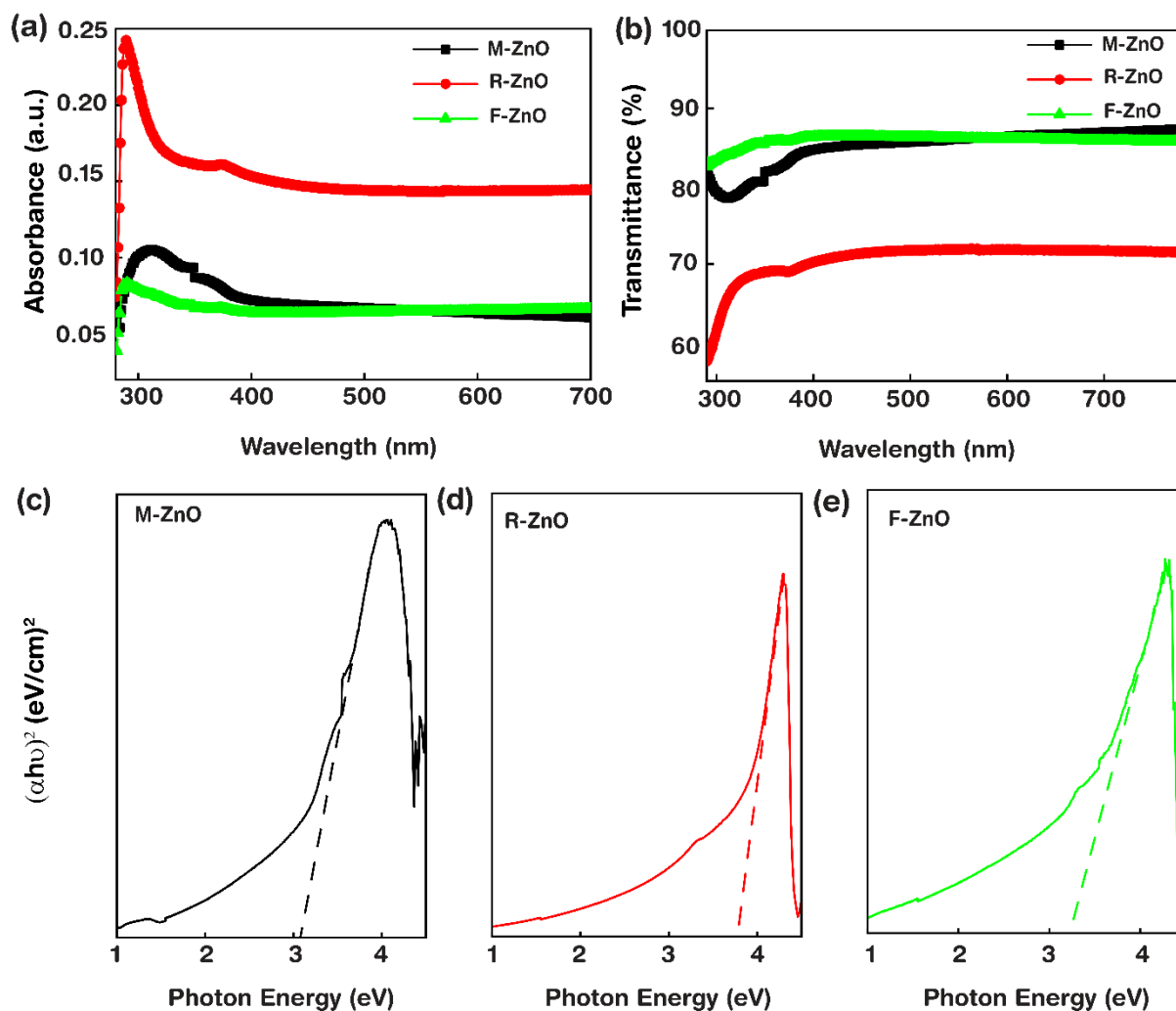
Figure 4: [(a)] transmittance spectrum [(b)] Absorbance spectra and band gap [(c-e)] of M-ZnO, R-ZnO and F-ZnO

2.4. XPS analysis for defect estimation

XPS analysis is further done to determine the presence of surface defects. Figure 5 demonstrates the comparison O 1s region of the XPS spectra of various morphologies of ZnO (a) R-ZnO, (b) M-ZnO and (c) F-ZnO. Previous studies have reported that the peak around ~530.05eV (O1) is due to oxygen in the Zn-O matrix, the peaks centered around~ 531.06~531.58 eV (O_2) generally originates from the surface defects in the ZnO structure especially oxygen vacancies. After gaussian fitting of peaks for each sample, the total areal percentage clearly indicated the higher presence of defects arising from the oxygen vacancies in ZnO porous microspheres (58.2%) is highest as compared to flower-like ZnO (32.2%) and ZnO nanorods (20.2%). This result confirms the proposed reason for higher wettability in porous microspheres than flower and rod morphologies.
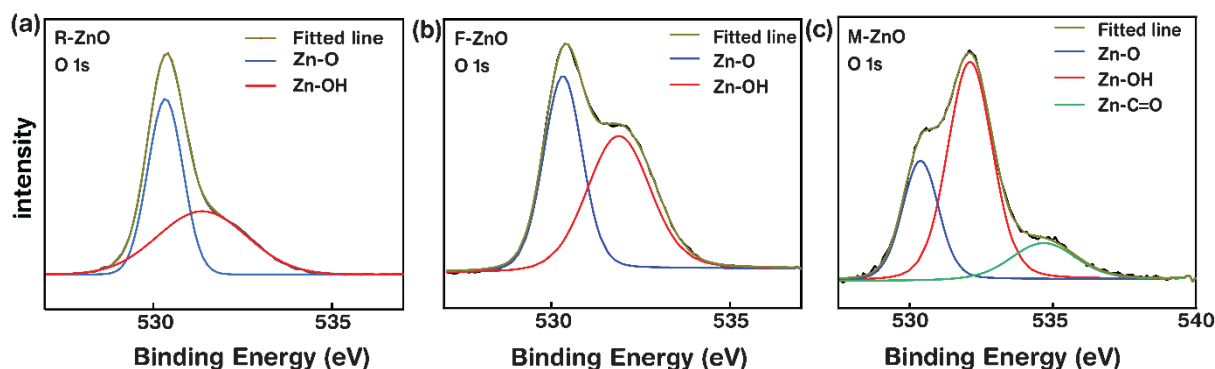
Figure 5: XPS spectra of deconvoluted O 1s spectrum of various morphologies of ZnO (a) R-ZnO; (b) F-ZnO and (c) M-ZnO.

3. Conclusion

We report self-cleaning microsphere ZnO(M-ZnO), nanorod ZnO (R-ZnO) and flower ZnO (F-ZnO) morphology developed by hydrothermal process on a glass substrate at ambient condition for anti-soiling of PV application. The structural and morphological properties were studied by X-ray diffraction (XRD) and field emission scanning microscopy (FESEM). The optical and wetting properties were investigated by UV-Vis spectrophotometer and water contact angle measurement respectively. Stable morphologies were obtained even after undergoing aging with post-annealing at 350°C on the glass substrate. Single crystal rod had diameter of 20 nm which changed to 5-7µm for flow structure. M-ZnO behaved as super hydrophilic as it had WCA of 2.8^0 which was lowest compared R-ZnO and F-ZnO having WCA of 20.2°, 11.19° respectively. M-ZnO had a bandgap of 3.1eV and more than 80% average visible (380-780 nm) transparency. Hydrophilic R-ZnO and F -ZnO had optical band gap of 3.6eV and 3.3ev respectively which supports their use in self-cleaning application.

4. Experiments

4.1. Material synthesis

4.1.1. Synthesis of ZnO rods (R-ZnO) and flower-like structure (F-ZnO)
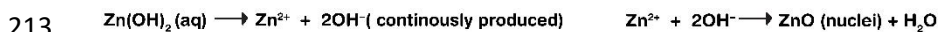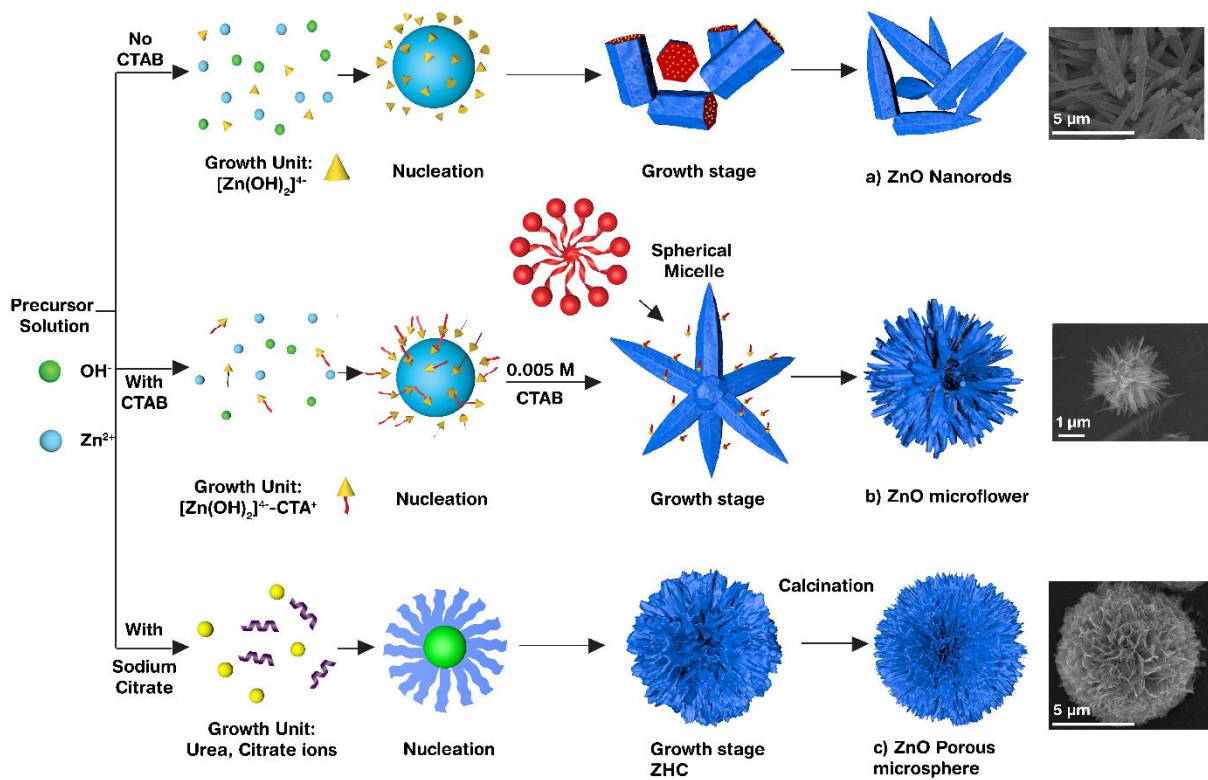
All chemicals were analytical grade and were used as purchased (sigma Aldrich) without any further purification process.

For the synthesis of flower-like ZnO microstructure (F-ZnO), 50 mL of (Zn $(NO_3)_2.H_2O$ (0.2M) transparent solution was steadily added to 50 mL of a transparent solution of 1.2M NaOH and 0.01 M of CTAB in an ice bath under vigorous stirring in an ice bath for 1 hour. The resulting solution was transferred in a 100 mL capacity autoclave with a Teflon liner and maintained at 90 °C for 5 hours. After the hydrothermal reaction was complete, the autoclave was left to cool down until room temperature. The white precipitate obtained was harvested by centrifugation and then thoroughly washing with distilled water and ethanol several times. The final white product was dried at 80°C in air

199   for 10 hours. The same experiment as mentioned above was repeated for the synthesis of ZnO microrods

200   (R-ZnO) in the absence of CTAB.

201   For the synthesis of ZnO microspheres, hydrothermal reaction with subsequent calcination was

202   conducted. In a typical synthesis process, an Optimized ratio of Zn $(NO_3)_2.H_2O$, urea $(CO(NH_2)_2)$ and

203   trisodium citrate $(Na_3C_6H_5O_7)$ in a ratio of 1:1:0.1 were steadily dissolved in 100 mL deionized water

204   under vigorous stirring to form a transparent solution. The resulting mixture was transferred into a

205   Teflon-lined stainless-steel autoclave and maintained at hydrothermal temperature 120°C for 5h. After

206   the hydrothermal reaction was complete the autoclave was left to cool down until room temperature.

207   The precipitate was harvested by centrifugation and was washed thoroughly with deionized water and

208   ethanol several times. The obtained white precipitate was dried at 80°C in air for 10 hours to obtain the

209   zinc carbonate hydroxide (ZHC), precursors. Further, for the synthesis of porous ZnO microspheres,

210   the as-obtained ZHC precursors were calcined at 500°C in CVD furnace for 2 h. After cooling the

211   system to room temperature, the final product was collected. Details of growth and formation

212   mechanism of nanorods, flower-like and porous microsphere of ZnO are shown in Figure 6.

213    $Zn(OH)_2 (aq) \longrightarrow Zn^{2+} + 2OH^-$ (continously produced) $Zn^{2+} + 2OH^- \longrightarrow ZnO$ (nuclei) + H_2O

214   Figure 6. Schematic of material synthesis (a) Nanorods (b) Flower-like and (c) Microsphere

215

216

4.2. Development of ZnO microstructure thin films

The deposition of the ZnO microstructures onto the glass substrate was carried out by using the drop-casting method. Before applying the material, the glass substrates were carefully washed for 50 mins in boiling diluted sulfuric acid (1:10 v/v) and rinsed thoroughly with deionized water, acetone and ethanol several times. The as-prepared ZnO samples were dissolved in DI water (0.5 weight: percent) and ultrasonicated and finally the solution was drop cast onto the surface of the glass substrate placed on a hot plate (100 °C). The film was dried by evaporating out the solvent and was subjected to post-annealing at 350 °C for 2 hrs. After completing the fabrication of the device, it was subjected to various characterizations.

4.3. Material Characterization

The crystal phases of the materials were determined by X-ray powder diffraction (**XRD**) using a Bruker D8 ADVANCE diffractometer with Cu Kα radiation and were matched the standard values using the Joint committee on powder diffraction standards (JCPDS) Database. The morphology of the sample was obtained using JSM-7600F, JEOL field emission scanning electron microscopy (**FE-SEM**). **Raman spectroscopy** analysis was carried out to evaluate structural defects and various modes in the prepared sample and the spectrum was recorded using an Alpha 300 M confocal micro-Raman spectrometer equipped with a YAG laser (532 nm). Further, Optical properties were analyzed by studying the **Photoluminescence (PL) spectrum** recorded at room temperature using a Fluorimeter (FS-2, Scinco) equipped with Xe-arc lamp having an excitation wavelength of 350 nm. **UV-Vis spectroscopy** analysis was carried out to evaluate the bandgap and the transmission properties of the prepared samples with the help of LAMBDA 1050 UV/Vis/NIR Spectrophotometer. Finally, in order to understand the wettability property of these materials and surface energy which is an essential parameter for self-cleaning application in solar panels, **contact angle measurement** was conducted by using contact angle meter (optical tensiometer).

Author Information

*Corresponding author (s): a.ghosh@exeter.ac.uk

ORCID

Dr. Aritra Ghosh: 0000-0001-9409-7592

References

(1)   Toth, S.; Muller, M.; Miller, D. C.; Moutinho, H.; To, B.; Micheli, L.; Linger, J.; Engtrakul, C.; Einhorn, A.; Simpson, L. Soiling and Cleaning: Initial Observations from 5-Year Photovoltaic Glass Coating Durability Study. *Sol. Energy Mater. Sol. Cells* **2018**, *185* (December 2017), 375–384. https://doi.org/10.1016/j.solmat.2018.05.039.

(2)   Piedra, P. G.; Llanza, L. R.; Moosmüller, H. Optical Losses of Photovoltaic Modules Due to Mineral Dust Deposition: Experimental Measurements and Theoretical Modeling. *Sol. Energy* **2018**, *164* (February), 160–173. https://doi.org/10.1016/j.solener.2018.02.030.

(3)   Sya, A.; Pandey, A. K.; Adzman, N. N.; Abd, N. Advances in Approaches and Methods for Self-Cleaning of Solar Photovoltaic Panels. **2018**, *162* (November 2017), 597–619. https://doi.org/10.1016/j.solener.2017.12.023.

(4)   Midtdal, K.; Jelle, B. P. Self-Cleaning Glazing Products: A State-of-the-Art Review and Future Research Pathways. *Sol. Energy Mater. Sol. Cells* **2013**, *109* (7465), 126–141. https://doi.org/10.1016/j.solmat.2012.09.034.

(5)   Zuo, Z.; Gao, J.; Liao, R.; Zhao, X.; Yuan, Y. A Novel and Facile Way to Fabricate Transparent Superhydrophobic Film on Glass with Self-Cleaning and Stability. *Mater. Lett.* **2019**, *239*, 48–51. https://doi.org/10.1016/j.matlet.2018.12.059.

(6)   Wang, Y.; Jiang, T.; Meng, D.; Yang, J.; Li, Y.; Ma, Q.; Han, J. Fabrication of

272   Nanostructured CuO Films by Electrodeposition and Their Photocatalytic Properties.

273   *Appl. Surf. Sci.* **2014**, *317*, 414–421. https://doi.org/10.1016/j.apsusc.2014.08.144.

274   (7)   Jiang, T.; Wang, Y.; Meng, D.; Wu, X.; Wang, J.; Chen, J. Controllable Fabrication of

275   CuO Nanostructure by Hydrothermal Method and Its Properties. *Appl. Surf. Sci.* **2014**,

276   *311*, 602–608. https://doi.org/10.1016/j.apsusc.2014.05.116.

277   (8)   Jang, G. G.; Smith, D. B.; Polizos, G.; Collins, L.; Keum, J. K.; Lee, D. F. Transparent

278   Superhydrophilic and Superhydrophobic Nanoparticle Textured Coatings:

279   Comparative Study of Anti-Soiling Performance. *Nanoscale Adv.* **2018**, *1* (3), 1249–

280   1260. https://doi.org/10.1039/c8na00349a.

281   (9)   Chen, Q.; Wang, Y.; Zheng, M.; Fang, H.; Meng, X. Nanostructures Confined Self-

282   Assembled in Biomimetic Nanochannels for Enhancing the Sensitivity of Biological

283   Molecules Response. *J. Mater. Sci. Mater. Electron.* **2018**, *29* (23), 19757–19767.

284   https://doi.org/10.1007/s10854-018-0101-2.

285   (10)   Jang, G. G.; Smith, D. B.; Polizos, G.; Collins, L.; Keum, J. K.; Lee, D. F. Nanoscale

286   Advances Transparent Superhydrophilic and Superhydrophobic Nanoparticle Textured

287   Coatings : Comparative Study of Anti-Soiling Performance †‡. **2019**, 1249–1260.

288   https://doi.org/10.1039/c8na00349a.

289   (11)   Nishimoto, S.; Bhushan, B. RSC Advances Bioinspired Self-Cleaning Surfaces With.

290   **2013**, 671–690. https://doi.org/10.1039/c2ra21260a.

291   (12)   Stieberova, B.; Zilka, M.; Ticha, M.; Freiberg, F.; Caramazana-gonza, P.; Mckechnie,

292   J.; Lester, E. Application of ZnO Nanoparticles in a Self-Cleaning Coating on a Metal

293   Panel: An Assessment of Environmental Bene Fi Ts. **2017**.

294   https://doi.org/10.1021/acssuschemeng.6b02848.

295   (13)   Sonker, R. K.; Yadav, B. C.; Gupta, V.; Tomar, M. Fabrication and Characterization of

296   ZnO-TiO 2 -PANI (ZTP) Micro/Nanoballs for the Detection of Flammable and Toxic

Gases. *J. Hazard. Mater.* **2019**, *370* (September 2018), 126–137.

https://doi.org/10.1016/j.jhazmat.2018.10.016.

(14)   Wang, Z. jun; Song, H.; Pang, H.; Ning, Y.; Dao, T. D.; Wang, Z.; Chen, H.; Weng,

Y.; Fu, Q.; Nagao, T.; et al. Photo-Assisted Methanol Synthesis via CO 2 Reduction

under Ambient Pressure over Plasmonic Cu/ZnO Catalysts. *Appl. Catal. B Environ.*

2019, *250* (March), 10–16. https://doi.org/10.1016/j.apcatb.2019.03.003.

(15)   Bu, I. Y. Y. Interconnected ZnO Branches as an Effective Electron Transfer Layer in

Perovskite Solar Cells. *Optik (Stuttg).* **2019**, *182* (December 2018), 32–36.

https://doi.org/10.1016/j.ijleo.2018.12.157.

(16)   Van De Loo, B. W. H.; Macco, B.; Melskens, J.; Beyer, W.; Kessels, W. M. M. Silicon

Surface Passivation by Transparent Conductive Zinc Oxide. *J. Appl. Phys.* **2019**, *125*

(10). https://doi.org/10.1063/1.5054166.

(17)   Tao, K.; Yi, H.; Tang, L.; Wu, J.; Wang, P.; Wang, N.; Hu, L.; Fu, Y.; Miao, J.;

Chang, H. Piezoelectric ZnO Thin Films for 2DOF MEMS Vibrational Energy

Harvesting. *Surf. Coatings Technol.* **2019**, *359* (August 2018), 289–295.

https://doi.org/10.1016/j.surfcoat.2018.11.102.

(18)   Orak, I.; Kocyigit, A.; Turut, A. The Surface Morphology Properties and Respond

Illumination Impact of ZnO/n-Si Photodiode by Prepared Atomic Layer Deposition

Technique. *J. Alloys Compd.* **2017**, *691*, 873–879.

https://doi.org/10.1016/j.jallcom.2016.08.295.

(19)   Caglar, Y.; Caglar, M.; Ilican, S.; Aksoy, S.; Yakuphanoglu, F. Effect of Channel

Thickness on the Field Effect Mobility of ZnO-TFT Fabricated by Sol Gel Process. *J.*

Alloys Compd. **2015**, *621*, 189–193. https://doi.org/10.1016/j.jallcom.2014.09.190.

(20)   Meng, P.; Gu, S.; Wang, J.; Hu, J.; He, J. Improving Electrical Properties of Multiple

Dopant ZnO Varistor by Doping with Indium and Gallium. *Ceram. Int.* **2018**, *44* (1),

322   1168–1171. https://doi.org/10.1016/j.ceramint.2017.07.173.

323   (21)   Chen, R.; Wan, Y.; Wu, W.; Yang, C.; He, J. H.; Cheng, J.; Jetter, R.; Ko, F. K.; Chen,

324   Y. A Lotus Effect-Inspired Flexible and Breathable Membrane with Hierarchical

325   Electrospinning Micro/Nanofibers and ZnO Nanowires. *Mater. Des.* **2019**, *162*, 246–

326   248. https://doi.org/10.1016/j.matdes.2018.11.041.

327   (22)   Shaik, U. P.; Purkayastha, D. D.; Krishna, M. G.; Madhurima, V. Nanostructured Zn

328   and ZnO Nanowire Thin Films for Mechanical and Self-Cleaning Applications. *Appl.*

329   *Surf. Sci.* **2015**, *330*, 292–299. https://doi.org/10.1016/j.apsusc.2015.01.027.

330   (23)   Guo, M.; Diao, P.; Cai, S. Highly Hydrophilic and Superhydrophobic ZnO Nanorod

331   Array Films. *Thin Solid Films* **2007**, *515* (18), 7162–7166.

332   https://doi.org/10.1016/j.tsf.2007.03.038.

333   (24)   Li, H.; Yu, S.; Hu, J.; Liu, E. A Robust Superhydrophobic Zn Coating with ZnO

334   Nanosheets on Steel Substrate and Its Self-Cleaning Property. *Thin Solid Films* **2018**,

335   *666* (September), 100–107. https://doi.org/10.1016/j.tsf.2018.09.019.

336   (25)   Zuo, Z.; Gao, J.; Liao, R.; Zhao, X.; Yuan, Y. A Novel and Facile Way to Fabricate

337   Transparent Superhydrophobic Film on Glass with Self-Cleaning and Stability. *Mater.*

338   *Lett.* **2019**, *239*, 48–51. https://doi.org/10.1016/j.matlet.2018.12.059.

339   (26)   Moafi, H. F.; Shojaie, A. F.; Zanjanchi, M. A. Photocatalytic Self-Cleaning Properties

340   of Cellulosic Fibers Modified by Nano-Sized Zinc Oxide. *Thin Solid Films* **2011**, *519*

341   (11), 3641–3646. https://doi.org/10.1016/j.tsf.2011.01.347.

342   (27)   Shaban, M.; Zayed, M.; Hamdy, H. Nanostructured ZnO Thin Films for Self-Cleaning

343   Applications. *RSC Adv.* **2017**, *7* (2), 617–631. https://doi.org/10.1039/c6ra24788a.

344   (28)   Pesika, N. S.; Hu, Z.; Stebe, K. J.; Searson, P. C. Quenching of Growth of ZnO

345   Nanoparticles by Adsorption of Octanethiol. *J. Phys. Chem. B* **2002**, *106* (28), 6985–

346   6990. https://doi.org/10.1021/jp0144606.

347   (29)   Chen, Y.; Zhang, C.; Huang, W.; Yang, C.; Huang, T.; Situ, Y.; Huang, H. Surface &

348   Coatings Technology Synthesis of Porous ZnO / TiO 2 Thin Fi Lms with

349   Superhydrophilicity and Photocatalytic Activity via a Template-Free Sol – Gel

350   Method. *Surf. Coat. Technol.* **2014**, *258*, 531–538.

351   https://doi.org/10.1016/j.surfcoat.2014.08.042.

352   (30)   Mozumder, M. S.; Mourad, A. H. I.; Pervez, H.; Surkatti, R. Recent Developments in

353   Multifunctional Coatings for Solar Panel Applications: A Review. *Sol. Energy Mater.*

354   *Sol. Cells* **2019**, *189* (September 2018), 75–102.

355   https://doi.org/10.1016/j.solmat.2018.09.015.

356   (31)   He, G.; Lu, S.; Xu, W.; Ye, P.; Liu, G.; Wang, H.; Dai, T. Stable Superhydrophobic

357   Zn/ZnO Surfaces Fabricated via Electrodeposition on Tin Substrate for Self-Cleaning

358   Behavior and Switchable Wettability. *J. Alloys Compd.* **2018**, *747*, 772–782.

359   https://doi.org/10.1016/j.jallcom.2018.03.108.

360   (32)   Cho, K. L.; Liaw, I. I.; Wu, A. H. F.; Lamb, R. N. Influence of Roughness on a

361   Transparent Superhydrophobic Coating. *J. Phys. Chem. C* **2010**, *114* (25), 11228–

362   11233. https://doi.org/10.1021/jp103479k.

363   (33)   Ebert, D.; Bhushan, B. Transparent, Superhydrophobic, and Wear-Resistant Coatings

364   on Glass and Polymer Substrates Using SiO2, ZnO, and ITO Nanoparticles. *Langmuir*

365   **2012**, *28* (31), 11391–11399. https://doi.org/10.1021/la301479c.

366   (34)   Karunakaran, R. G.; Lu, C. H.; Zhang, Z.; Yang, S. Highly Transparent

367   Superhydrophobic Surfaces from the Coassembly of Nanoparticles ($\leq$ 100 Nm).

368   *Langmuir* **2011**, *27* (8), 4594–4602. https://doi.org/10.1021/la104067c.

369

370

371

372

373

374 ## Table of Contents

Water

Superhydrophilic ZnO-coating

Dirt Particles

Clean Surface

PV System/ BIPV/ Window

ZnO Nanorods — 5 μm

ZnO Microflower — 1 μm

ZnO Porous Microflower — 5 μm

375